WIRELESS COMMUNICATIONS AND MOBILE COMPUTING
Wirel. Commun. Mob. Comput. 2009; **9**:1–20
Published online 7 October 2008 in Wiley InterScience
(www.interscience.wiley.com) DOI: 10.1002/wcm.671

Analysis of multi-user detection of multi-rate transmissions in multi-cellular CDMA

Besma Smida[1*,†] and Sofiène Affes[2]
[1]*School of Engineering and Applied Sciences, Harvard University, Cambridge, U.S.A.*
[2]*INRS-EMT, University of Quebec, Montreal, Canada*

Summary

In this paper, we address the issue of multi-user receiver design in realistic multi-cellular and multi-rate CDMA systems based on performance analysis. We consider the multi-user detection (MUD) technique, denoted interference subspace rejection (ISR), because it offers a wide range of canonic suppression modes that range in performance and complexity between interference cancellers and linear receivers. To further broaden our study, we propose a modified ISR scheme called hybrid ISR to cope better with multi-rate transmissions. The performance analysis, which is based on the Gaussian assumption (GA) and validated by simulations, takes into account data estimation errors, carrier frequency mismatch, imperfect power control, identification errors of time-varying multipath Rayleigh channels and intercell interference. This analysis enables us to optimize the selection of the MUD mode for multi-rate transmissions in different operating conditions. The effectiveness of interference cancellation is indeed investigated under different mobile speeds, numbers of receiving antennas, near-far situations, channel estimation errors, and out-cell to in-cell interference ratios. This investigation suggests that the out-of-cell interference, the residual in-cell interference, the noise enhancement as well as low mobility favor the simplest MUD modes as they offer the best performance/complexity tradeoffs. Copyright © 2008 John Wiley & Sons, Ltd.

KEY WORDS: CDMA; multi-user detection; multi-cellular; multi-rate

1. Introduction

The 'third-generation and beyond' wireless communication systems must be able to offer wireless transport for a variety of information sources with inherently different data rates, including voice, data, and image. In such multi-cellular and mixed-rate traffic scenarios, the conventional receiver fails to demodulate transmissions from the weak low-rate users. It is therefore imperative to use more sophisticated multi-user CDMA receivers with better interference cancellation capabilities [1]. One open area is the design of spectrum-efficient multi-user receivers that will enable the future upgrade of current wireless networks beyond third generation. Transceivers selected for early implementation need to achieve high spectrum efficiency in realistic propagation channels while being well adapted to multi-cellular and multi-rate CDMA systems. In realistic wireless systems the performance of multi-user receivers will not be affected by the thermal noise only, but it will be damaged by various interference sources such as the residual incell interference and

*Correspondence to: Besma Smida, School of Engineering and Applied Sciences, Harvard University, Cambridge, U.S.A.
[†]E-mail: bsmida@seas.harvard.edu

Copyright © 2008 John Wiley & Sons, Ltd.

the intercell interference. The residual incell interference is due to wrong tentative data decisions, channel estimation errors, and power control errors in the interference cancellation process. On the other hand the intercell interference that originates from users outside the cell of interest may account for up to 60% of the total interference in some scenarios [2]. Hence, if interference cancellation is successful within the cell, the performance of the system will be limited by the interference from the other cells. Yet, little has been done to take the residual incell interference and the intercell interference into account in the system design.

So far, several multi-user receivers originally proposed for single-rate transmission have been investigated for multi-rate CDMA systems, including the linear and non-linear multi-user detectors [3–8]. Hybrid receivers that combine different multi-user detection (MUD) techniques were also considered for multi-rate CDMA [9–12]. Most of these studies have focused on the single-cell environment. Some works have investigated the effect of the out-cell interference on the performance of multi-user receivers, but they all assume single-rate transmission and perfect knowledge of the propagation channel [13–15]. To the authors' best knowledge, no investigations that take into account the data, channel and power control estimation errors, and the intercell interference are available in the literature.

This paper considers an alternative MUD technique, denoted interference subspace rejection (ISR). This technique has been proposed for single-rate DS-CDMA [16] and it has been shown to provide attractive perforamnce/complexity tradeoffs. ISR offers different modes (referred to as canonic in the following) that range in performance and complexity between IC detectors and linear receivers.[‡] At the low end, ISR reconstructs the interference from channel and data hard decision estimates, then suppresses it like IC methods. Compared to the linear receivers at the high end, ISR implements nulling along different interference subspace decompositions. Each canonic mode characterizes the interference vector in a different way and accordingly suppresses it. To broaden our study, we propose a modified ISR scheme called hybrid ISR that presumably adapts better to multi-rate transmissions. Indeed, instead of detecting all active users targeted for suppression with the same canonic ISR mode, hybrid ISR splits them into several groups based on their data rate using the new block data structure, then applies different canonic ISR modes for their nulling. This new approach offers an even wider range of suppression modes. In addition, the evaluation of hybrid ISR is oriented toward an implementation in a future, real-world wireless system operating in a multi-rate environment. Indeed this analysis takes into account data estimation errors, carrier frequency mismatch, imperfect power control, identification errors of time-varying multipath Rayleigh channels and, intercell interference. With reference to the previous work [16], we summarize our main contributions as follows:

- We derive a data block processing structure well suited to multi-rate data traffic. We model both the high-rate and low-rate users as serval virtual users. This data model enables us to increase the precessing window and hence reduce the noise enhancement. In addition, it permits the implementation of a multi-user receiver that simultaneously supports multi-code, variable spreading factor, and different modulation formats.
- We propose a hybrid ISR receiver that simultaneously rejects the interference from the high-rate and low-rate users with different canonic ISR modes. Indeed, in Reference [16], a MUD technique was proposed for the mixed-rate scenario referred to as Group/Hybrid detection. This technique constructs two interference subspaces (inter-group and intra-group) and then successively suppresses the interference generated from each of them. This double projection increases noise enhancement, which is a performance degradation key factor in a multi-cellular environment. In this paper, in contrast to the former approach, we null a combined and unique interference subspace in a single processing step and hence significantly reduce the computational complexity. We simultaneously reject the interference from the high-rate and low-rate users with different canonic ISR modes. This new approach offers an even wider range of suppression modes.
- We derive a link/system-level performance analysis of multi-cellular and multi-rate CDMA with hybrid ISR. This analysis, which is based on the Gaussian assumption (GA), is validated by simulations. We exploit the analysis results of single-rate ISR recently

[‡] ISR offers a unifying framework for MUD that encompasses almost all existing non-linear and linear MUD receivers with much more variants that offer improved performance/compexlity tradeoffs. ISR can implement ZF- or MMSE-based interference suppression as well as a combination of both. Here, we select ZF-type ISR for its analytical tractability.

Copyright © 2008 John Wiley & Sons, Ltd.

DOI: 10.1002/wcm

developed in Reference [17] at the link-level and extend them to hybrid ISR. Additionally, we broaden the scope of the analysis to include carrier frequency mismatch, imperfect power control, identification errors of time-varying multipath Rayleigh channels, and intercell interference. Using the link-level performance analysis, we will also propose a simple computation procedure to evaluate the capacity in terms of number of users per cell and total throughput in a multi-rate multi-cellular context.

- We address the general problem of how to assign modes to the different groups of users so as to maximize the total multi-cellular system throughput, given an operating condition (*i.e.*, propagation environment, multi-rate distribution). Based on the link/system-level performance analysis, we design an efficient suppression mode strategy for multi-cellular and multi-rate CDMA, that strives to maximize throughput while containing the extra computational cost.

The organization of this paper is as follows: In Section 2 we present a multi-rate data block model. In Section 3 we introduce the new hybrid ISR before we derive the link/sytem-level performance analysis and propose a mode assignment strategy in Section 4. We evaluate the improved performance/complexity tradeoffs offered by hybrid multi-rate ISR in Section 5. Finally, we conclude in Section 6.

2. Data Model for Multi-Rate CDMA

We consider the uplink of an asynchronous multi-cellular multi-rate CDMA system where each base station is equipped with M receiving antennas. The system consists of U in-cell active users that transmit data with different spreading factors and different modulation formats (extension to the multi-code scheme is ad hoc). The data $b_n^u \in C_{\mathcal{M}_u}$ for a user assigned the index u is $\mathcal{M}_u$-PSK modulated and differentially[§] encoded at rate $1/T_u$, where T_u is the symbol duration and $C_{\mathcal{M}_u} = \{\ldots, e^{\frac{j2\pi m}{\mathcal{M}_u}}, \ldots\}$, $m \in \{0, \ldots, \mathcal{M}_u - 1\}$. The data sequence is then spread by a long spreading code $c^u(t)$. The spreading factor L_u is defined as the ratio of the symbol duration T_u and the chip duration T_c. We convert the variable spreading factor scenario into a single spreading factor scenario where each high data-rate user is equivalent to Q_u virtual low data-rate users. The spreading sequence for the kth virtual user (kth symbol) of the uth user is

$$c^{u,k}(t) = \begin{cases} c^u(t) & \text{for} \quad (k-1)T_u \le t < kT_u \\ 0 & \text{else} \end{cases} \tag{1}$$

We consider a multipath Rayleigh fading channel with P resolvable paths and delay spread $\Delta\tau$. We assume that the channel parameters (*i.e.*, delays, power, fade magnitudes, and phases) vary slowly and neglect their variation over the largest symbol duration. This allows for data processing in successive blocks of Q_u symbols.

Regardless of the data-rate, the receiver implements down conversion, matched pulse filtering and chip-rate sampling followed by framing the observation into overlapping blocks of constant length of N_P chips. As shown in Figure 1(a), the resulting processing block duration $T_P = N_P T_c$ is equal to $T_{\max} + \bar{\Delta}\tau$. The processing period $T_{\max} = Q_u T_u$, which is also equal to the maximum spreading factor $L_{\max} \times T_c$, contains integer numbers of symbols Q_u targeted for detection in each block for user u. The frame overlap $\bar{\Delta}\tau < T_{\max}$, which is larger than the delay spread to allow multipath tracking [19], comprises $Q_{\bar{\Delta},u} = \lceil \bar{\Delta}\tau / T_u \rceil$ symbols for user u and translates into a maximum temporal expansion of each symbol within the processing block from T_u to $T_u + \bar{\Delta}\tau$ at the receiver (see dark grey areas in Figure 1(a)). Hence we obtain the $M \times N_P$ matched-filter observation matrix [16]:

$$\mathbf{Y}_n = [Y_n(0), Y_n(T_c), \ldots, Y_n((N_P - 1)T_c)] \tag{2}$$

where

$$Y_n(t) = \frac{1}{T_c} \int_{D_\phi} X(nT_{\max} + t + t')\phi(t')\,\mathrm{d}t' \tag{3}$$

$X(t)$ is the observation vector received by the antenna array and D_ϕ is the temporal support of the chip pulse $\phi(t)$. $\mathbf{Y}_n$ can be expressed as

$$\mathbf{Y}_n = \sum_{u=1}^{U} \psi_n^u \mathbf{Y}_n^u + \mathbf{N}_n^{th} \tag{4}$$

where each user u contributes its user-observation matrix $\mathbf{Y}_n^u$ scaled by its total received power $(\psi_n^u)^2$ and where the base-band preprocessed thermal noise contributes $\mathbf{N}_n^{th}$. Note that we consider a closed-loop power-controlled system to ensure an

[§] We can also use pilot symbols for coherent modulation and detection [18], but that is beyond the scope of this paper.

Copyright © 2008 John Wiley & Sons, Ltd.

DOI: 10.1002/wcm

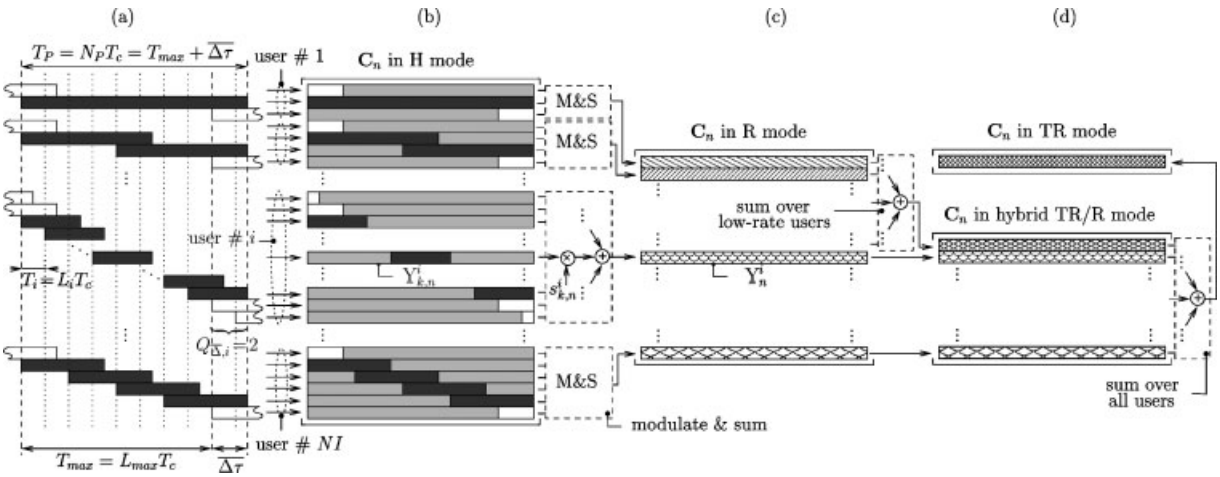

Fig. 1. Signal structure of the data block and construction of the null constraints of $\mathbf{C}_n$ for the canonic ISR modes (H, R, and TR) and the hybrid TR/R mode: desired symbols to be extracted are in dark grey, edge symbols from adjacent frames are in white, zero elements are in light grey. We construct $\mathbf{C}_n^{d,k}$ by excluding $s^d_{k,n}\underline{Y}^d_{k,n}$ from the various summations in the TR, R, and TR/R modes.

equal received power for all users having the same modulation/spreading factor combination. In the following, we assume that the base station targets NI interfering users (presumably with high data-rate and/or strong power) for joint suppression among the U active users (*e.g.*, all incell users). Using Equation (4) and defining a vector $\underline{V}$ as matrix $\mathbf{V}$ reshaped columwise, we can rewrite the matched-filtering observation matrix for the desired user assigned index $d \in \{1, \ldots, NI\}$ with respect to its kth symbol targeted for detection for $k = 0, \ldots, Q_d - 1$ in the following vector form [16]:

$$\underline{Y}_n = \sum_{i=1}^{NI} \sum_{k=-Q_{\bar{\Delta},i}}^{Q_i+Q_{\bar{\Delta},i}-1} s_n^{i,k} \underline{Y}^i_{k,n} + \underline{N}_n \tag{5}$$

$$= \underbrace{s_n^{d,k}\underline{Y}^d_{k,n}}_{\text{desired signal}} + \underbrace{\sum_{\substack{i=1 \\ i\neq d}}^{NI} \psi^i_n \underline{Y}^i_n}_{\underline{I}^d_{\text{MAI},n}} + \underbrace{\sum_{\substack{k'=-Q_{\bar{\Delta},d} \\ k'\neq k}}^{Q_d+Q_{\bar{\Delta},d}-1} s_n^{d,k'}\underline{Y}^d_{k',n}}_{\underline{I}^{d,k}_{\text{ISI},n}} + \underline{N}_n \tag{6}$$

$$= s_n^{d,k}\underline{Y}^d_{k,n} + \underline{I}^{d,k}_n + \underline{N}_n \tag{7}$$

where $s_n^{d,k} = \psi^d_n b^d_{k,n}$ is the kth signal component and $\underline{Y}^d_{k,n}$ is the canonic user-observation vector due to the kth symbol. $\underline{I}^d_{\text{MAI},n}$ and $\underline{I}^{d,k}_{\text{ISI},n}$ are the multiple access interference and the inter-symbol interference to be suppressed with the respect to the kth symbol of user d. The noise vector $\underline{N}_n$ comprises the preprocessed thermal noise and the rest of the active users. Note that in Equation (5) the summation over the symbol index k ranges from $-Q_{\bar{\Delta},i}$ to $Q_i + Q_{\bar{\Delta},i} - 1$, instead of 1 to Q_i as calculated by the low-rate decorrelator (LDR) [4]. Due asynchronism and multipath propagation, the data block includes all the desired symbols to be extracted and the contribution from adjacent blocks, namely $Q_{\bar{\Delta},i}$ past symbols and $Q_{\bar{\Delta},i}$ future symbols.

As an alternative to the decomposition over symbols of Equation (5), the parametric data decomposition introduced in Reference [16] shows that we can separate the user-observation vector over contributions from the $N_f = MP$ diversity branches or fingers as

$$\underline{Y}_n = \sum_{i=1}^{NI} \sum_{f=1}^{N_f} \psi^i_n \zeta^i_{f,n} \underline{Y}^{i,f}_n + \underline{N}_n \tag{8}$$

where finger $f = (p-1)M + m$ denotes antenna $m \in 1, \ldots, M$ and propagation path $p \in 1, \ldots, P$, $\zeta^u_{f,l}$ stands for the corresponding propagation coefficient, and $\underline{Y}^{i,f}_n$ is the diversity-observation vector. The two decompositions of the user-observation vector (*i.e.*, over symbols or diversity branches) can be combined as follows:

$$\underline{Y}_n = \sum_{i=1}^{NI} \sum_{k=-Q_{\bar{\Delta},i}}^{Q_i+Q_{\bar{\Delta},i}-1} \sum_{f=1}^{N_f} \psi^i_n b^i_{nQ_i+k} \zeta^i_{f,n} \underline{Y}^{i,f}_{k,n} + \underline{N}_n \tag{9}$$

where $\underline{Y}^{i,f}_{k,n}$ is the canonic diversity-observation vector [16]. Hence, we can detail the structure of the

Copyright © 2008 John Wiley & Sons, Ltd.

DOI: 10.1002/wcm

interference $\underline{I}_n^{d,k}$ (introduced in Equation (5)) as

$$\underline{I}_n^{d,k} = \sum_{i=1}^{NI} \sum_{k'=-Q_{\bar{\Delta},i}}^{Q_i+Q_{\bar{\Delta},i}-1} \sum_{f=1}^{N_f} \psi_n^i b_{nQ_i+k'}^i \zeta_{f,n}^i \underline{Y}_{k',n}^{i,f} \delta_{d,i}^{k,k'}$$

$$= \sum_{i=1}^{NI} \sum_{k'=-Q_{\bar{\Delta},i}}^{Q_i+Q_{\bar{\Delta},i}-1} \sum_{f=1}^{N_f} \underline{Z}_{k',n}^{i,f} \delta_{d,i}^{k,k'} \tag{10}$$

where $\delta_{d,i}^{k,k'} = 0$ if $d = i$ and $k = k'$, and 1 otherwise, and

$$\underline{Z}_{k',n}^{i,f} = \psi_n^i b_{nQ_i+k'}^i \zeta_{f,n}^i \underline{Y}_{k',n}^{i,f} \tag{11}$$

The resulting decomposition permits the proposed multi-user receiver to combat both ISI and MAI and to efficiently detect multi-rate signals as explained in the next section.

3. Hybrid ISR for Multi-Rate CDMA

To summarize the ISR detection concept, we provide a geometric interpretation of some ISR canonic modes. In the general case, the total interference $\underline{I}_n^{d,k}$ is an unknown random vector which lies in an interference subspace spanned by a user-symbol-specific constraint matrix $\mathbf{C}_n^{d,k}$ with dimension that depends on the number of interference parameters estimated separately. The more interference parameters we estimate, the fewer dimensions N_c (number of constraints) are needed to characterize the interference subspace for suppression. However, the sensitivity of the suppression method to parameter estimation errors also increases. A number of alternative modes are available to construct the constraint matrix $\mathbf{C}_n^{d,k}$ [16] as illustrated in Figure 1. In Figure 1(b), the H (hypotheses) mode nulls the signal vector from each interfering symbol of each interferer by assigning a null-constraint column to each received edge (see white areas in Figure 1(b)) or desired (see dark grey areas in Figure 1(b)) symbol from each user after convolution with the propagation channel (see Figure 1(a)) and hence introduces robustness to symbol data estimation errors. The D (diversities) mode, not illustrated in Figure 1 because it requires a data decomposition over paths different from the one in Figure 1(a) based on symbols, nulls the signal vector from each interfering finger and hence gains additional robustness to channel estimation errors. A combination of the H and D modes, referred to as HD mode, results in a structure similar to the *path-by-path* decorrelator which provides robustness to channel and symbol data estimation errors. This mode will not be considered in the remainder of the paper due to its prohibitive complexity. In Figure 1(c), the R (realizations) mode nulls the signal vector of each interferer by assigning a null-constraint column to the data received from each user after symbol modulation and summation of the corresponding user's constraint columns in the H mode (see Figure 1(c)) and hence is less sensitive to power estimation errors. In Figure 1(d), the TR (total realizations) mode nulls the total interference vector by assigning a single null-constraint column to the total received data after summation of all constraint columns over users in the R mode and hence requires accurate estimation of all the channel and data parameters of the *NI* interferers. It is similar to the PIC detector, only it implements a more accurate nulling (projection) instead of subtraction.

In terms of computational complexity, the TR mode stands out as the least complex and the more practical ISR mode for implementation. Potential upgrade to the R mode can offer a relatively large performance gain (as illustrated later by simulations); however, it also requires a more than twofold increase in complexity. The HD mode, which is the most complex mode, offers even more computationally-expensive performance gains. In Table I, we provide estimates of the complexity for different items of ISR. The complexity of the ISR technique is mainly determined

Table I. Estimated complexity items for ISR. $\bar{\delta}(N_c) = 0$ if $N_c = 1$, and 1 otherwise. $L_{\bar{\Delta}} = \lceil \overline{\Delta\tau}/T_c \rceil$. $n_{ID} = 10$ if low Doppler, and 1 otherwise.

	Complexity items for ISR
Calculation of $\underline{Y}_{k,n}^d$	$ML_dL_{\bar{\Delta}}Q_dNI$
Reconstruction of $\mathbf{C}_n^{d,k}$	$M(2L_{\bar{\Delta}}^2/(Q_dL_d) + L_d)Q_dNI$
Projection $\Pi_n^{d,k}$	$4MN_c(L_d + L_{\bar{\Delta}})Q_dNI + \bar{\delta}(N_c)\left[2M(N_c^2/Q_d)N_PNI + (N_c^3/Q_d + N_c^2)NI\right]$
Estimation of $s_n^{d,k}$	$6M(L_d + L_{\bar{\Delta}})Q_dNI$
Channel identification	$\frac{1}{n_{ID}}(2ML_{\bar{\Delta}} + ML_{\bar{\Delta}}L)Q_dNI$

Copyright © 2008 John Wiley & Sons, Ltd.

DOI: 10.1002/wcm

by the number of users to be cancelled NI, and the total N_c imposed by the rejection mode. Hence, for a given multi-user system, increasing N_c will increase the complexity of the detection technique.

These observations prompt us to propose a hybrid ISR detection technique that provides a wider range of performance/complexity tradeoffs in multi-rate traffic. Instead of detecting all active users targeted for suppression with the same canonic ISR mode, hybrid ISR splits them into several groups based on their data rate, then applies different canonic ISR modes for their nulling. It simultaneously rejects the interference from the high-rate and low-rate users with different canonic ISR modes. As one example illustrated in Figure 1(d), a hybrid of the R and TR modes, referred to as TR/R, nulls the received data from each high-rate user and the total received data over all low-rate users by assigning, respectively, an individual null-constraint column to each high-rate user and a single null-constraint column to the remaining low-rate users after partial summation of the constraint columns in the R mode over the low-rate users only (see Figure 1(d)). It hence combines the robustness of the R mode with the computational efficiency of the TR mode (see simulation results in Section 5). More generally, this new hybrid approach offers a wider range of hybrid suppression modes. The hybrid constraint matrix will have the following form:

$$
\begin{aligned}
\hat{\mathbf{C}}_n^{d,k} = {} & \left[\sum_{i=1}^{N_{\mathrm{TR}}} \sum_{k'=-Q_{\bar{\Delta},i}}^{Q_i+Q_{\bar{\Delta},i}-1} \sum_{f=1}^{N_f} \hat{\psi}_n^i \hat{b}_{nQ_i+k'}^i \hat{\zeta}_{f,n}^i \underline{\hat{Y}}_{k',n}^{i,f} \delta_{d,i}^{k,k'} \right. \\
& \left\{ \ldots, \sum_{k'=-Q_{\bar{\Delta},i}}^{Q_i+Q_{\bar{\Delta},i}-1} \sum_{f=1}^{N_f} \hat{b}_{nQ_i+k'}^i \hat{\zeta}_{f,n}^i \underline{\hat{Y}}_{k',n}^{i,f} \delta_{d,i}^{k,k'}, \ldots \right\}_{i=N_{\mathrm{TR}}+1}^{N_{\mathrm{TR}}+N_R} \\
& \left\{ \ldots, \sum_{k'=-Q_{\bar{\Delta},i}}^{Q_i+Q_{\bar{\Delta},i}-1} \hat{b}_{nQ_i+k'}^i \underline{\hat{Y}}_{k',n}^{i,f} \delta_{d,i}^{k,k'}, \ldots \right\}_{(i,f)=(N_{\mathrm{TR}}+N_R+1,1)}^{(N_{\mathrm{TR}}+N_R+N_D,N_f)} \\
& \left\{ \ldots, \sum_{f=1}^{N_f} \hat{\zeta}_{f,n}^i \underline{\hat{Y}}_{k',n}^{i,f} \delta_{d,i}^{k,k'}, \ldots \right\}_{(i,k')=(N_{\mathrm{TR}}+N_R+N_D+1,-Q_{\bar{\Delta},i})}^{(N_{\mathrm{TR}}+N_R+N_D+N_H,Q_i+Q_{\bar{\Delta},i}-1)} \\
& \left. \left\{ \ldots, \underline{\hat{Y}}_{k',n}^{i,f}, \ldots \right\}_{(i,f,k')=(N_{\mathrm{TR}}+N_R+N_D+N_H+1,1,-Q_{\bar{\Delta},i})}^{(NI,N_f,Q_i+Q_{\bar{\Delta},i}-1)} \right]
\end{aligned}
\tag{12}
$$

where $\delta_{d,i}^{k,k'} = 0$ if $(i,k') = (d,k)$, and 1 otherwise. N_{TR}, N_R, N_D, N_H, and N_{HD} are the number of users in groups detected by the canonic modes TR, R, D, H, and HD, respectively. The total number of constraints is $N_c = 1 + N_R + N_D N_f + N_H(Q_i^h + 2Q_{\bar{\Delta},i}^h) + N_{\mathrm{HD}} N_f (Q_i^{hd} + 2Q_{\bar{\Delta},i}^{hd})$, where $Q_i^m + 2Q_{\bar{\Delta},i}^m$ is the number of symbols in the processing block of user i detected by mode m. Provided that an estimate of the constraint matrix $\hat{\mathbf{C}}_n^{d,k}$ is made available at the receiver, we can eliminate the total interference and yet achieve distortionless response to the desired signal by imposing the following constraints to the combiner:

$$
\begin{cases} \underline{W}_n^{d,k\,H} \underline{\hat{Y}}_{k,n}^d = 1 \\ \underline{W}_n^{d,k\,H} \hat{\mathbf{C}}_n^{d,k} = 0 \end{cases} \tag{13}
$$

The first constraint guarantees a distortionless response to the desired signal while the second directs a null to the total interference realization and thereby cancels it. Exploiting the general framework developed in Reference [16], the solution to the specific optimization problem in Equation (38) is the hybrid ISR combiner $\underline{W}_n^{d,k}$ given as follows:

$$
\mathbf{Q}_n = \left(\hat{\mathbf{C}}_n^H \hat{\mathbf{C}}_n \right)^{-1}, \quad \mathbf{\Pi}_n^{d,k} = \mathbf{I}_{N_T} - \hat{\mathbf{C}}_n \mathbf{Q}_n \hat{\mathbf{C}}_n^{d,kH},
$$

$$
\underline{W}_n^{d,k} = \frac{\Pi_n^{d,k} \underline{\hat{Y}}_{k,n}^d}{\underline{\hat{Y}}_{k,n}^{dH} \Pi_n^{d,k} \underline{\hat{Y}}_{k,n}^d} \tag{14}
$$

where $\mathbf{C}_n$ is formed by adding the contribution of the kth symbol of the desired user to the constraint matrix $\mathbf{C}_n^{d,k}$, $N_T = M \times N_P$ is the total space dimension, and $\mathbf{I}_{N_T}$ denotes an $N_T \times N_T$ identity matrix. We extract

Copyright © 2008 John Wiley & Sons, Ltd.

DOI: 10.1002/wcm

the kth signal component of the dth user as

$$\hat{s}_n^{d,k} = \underline{W}_n^{d,k^H} \underline{Y}_n \tag{15}$$

Such a hybrid multi-user detector adapts efficiently to multi-rate transmissions with mixed spreading factors and/or modulations (as well as multi-code). Note that, in Reference [16], a MUD technique for the mixed rate scenario was proposed and referred to as Group/Hybrid detection. This technique suggests the construction of two constraint matrices (inter-group and intra-group) and two different projectors, then projects the observation vector successively on each interference subspace. In this paper, in contrast to the former approach, we propose a unique hybrid constraint matrix and we null a combined and unique interference subspace in a single processing step and hence significantly reduce the computational complexity. We simultaneously reject the interference from the high-rate and low-rate users with different canonic ISR modes.

4. Detection Mode Assignment Strategy

The main feature of hybrid ISR is that it splits users into several groups based on their data-rate and power, then applies different canonic ISR modes for their nulling. A key element in this approach is the mode assignment strategy, *i.e.*, how to assign modes to the different groups of users so as to maximize the total multi-cellular system throughput, given an operating condition (*i.e.*, propagation environment, multi-rate distribution, complexity limit). Indeed, we notice that a potential upgrade to more robust detection modes will not only increase the complexity but also result in more severe noise enhancement. Indeed, even though higher-complexity modes are able to effectively suppress interference despite the estimation errors, their performance suffers from a problem known as noise enhancement. During the combining process, the noise and residual interference components[‖] in the received signal are also scaled by the combiner. This has been shown to result in greater noise and residual interference power. Note that in realistic cellular systems the background noise comes not only from the thermal noise but also from other sources such as intercell interference which can be relatively strong. Consequently, in the case where noise and residual interference are stronger than the total interference, the mode with higher complexity is likely to perform worse than the mode with lower complexity. It is therefore inefficient to apply a complex mode in an environment where it does not significantly outperform modes with lower complexity. To address this issue, we derive a link/system-level performance analysis of multi-cellular CDMA with hybrid ISR of multi-rate transmissions.

4.1. Link-Level Performance Analysis

This section is dedicated to the link-level performance analysis of the hybrid ISR receiver based on the GA. We exploit the analysis results of single-rate ISR recently developed in Reference [17] at the link-level and extend them to hybrid ISR. Additionally, we broaden the scope of the analysis to include carrier frequency mismatch, channel identification errors, and imperfect power control.

The post-combined signal can be formulated as

$$\hat{s}_n^{d,k} = \underline{W}_n^{d,k^H} \underline{Y}_n = \frac{\hat{\underline{Y}}_{k,n}^{d\ H} \underline{Y}_{k,n}^d}{\|\hat{\underline{Y}}_{k,n}^d\|^2} s_n^{d,k} + \delta_{\mathrm{MAI},n}^{d,k} + \delta_{\mathrm{ISI},n}^{d,k} + \underline{W}_n^{d,k^H} \underline{N}_n \tag{16}$$

where $\delta_{\mathrm{MAI},n}^{d,k}$ is the residual MAI and $\delta_{\mathrm{ISI},n}^{d,k}$ is the residual ISI. We assume here that the interference rejection residuals $\delta_{\mathrm{MAI},n}^{d,k}$ and $\delta_{\mathrm{ISI},n}^{d,k}$ are Gaussian random variables with zero mean. Hence, we only need to evaluate their variances. Note that the residuals would be null (*i.e.*, $\delta_{\mathrm{MAI},n}^{d,k} = \delta_{\mathrm{ISI},n}^{d,k} = 0$) if the reconstruction of the interference were perfect (*i.e.*, $\hat{\underline{I}}_{k,n}^d = \underline{I}_{k,n}^d$) and hence $\hat{s}_n^{d,k} = s_n^{d,k} + \underline{W}_n^{d,k^H} \underline{N}_n$ would be corrupted only by the residual noise, which is Gaussian with zero mean and variance

$$\mathrm{Var}\left[\underline{W}_n^{d,k^H} \underline{N}_n\right] = \bar{\kappa}\sigma_N^2 \tag{17}$$

where $\bar{\kappa} = \mathrm{E}[\|\underline{W}_n^{d,k}\|^2] = \frac{N_T}{N_T - Nc + 1}$ is a measure of the enhancement of the white noise compared to MRC ($\bar{\kappa} = 1$ for MRC) [20]. However, in practice the interference vector is reconstructed erroneously due to wrong tentative data decisions, channel estimation

[‖] The residual interference is due to wrong tentative data decisions, channel estimation errors, and power control errors.

Copyright © 2008 John Wiley & Sons, Ltd.

DOI: 10.1002/wcm

errors, and power control errors and hence $\hat{s}_n^{d,k}$ is further corrupted by non-null residual interference

The hybrid ISR combiner $\underline{W}_n^{d,k}$ satisfies the optimization property in Equation (13), thus

$$\underline{W}_n^{d,k^H}\hat{\mathbf{C}}_n^{d,k}=0 \implies \begin{cases} \displaystyle\sum_{i=1}^{N_{\mathrm{TR}}}\sum_{k'=-Q_{\bar{\Delta},i}}^{Q_i+Q_{\bar{\Delta},i}-1}\sum_{f=1}^{N_f}\underline{W}_n^{d,k^H}\hat{\psi}_n^i\hat{b}^i_{nQ_i+k'}\hat{\zeta}^i_{f,n}\underline{\hat{Y}}^{i,f}_{k',n}\delta^{k,k'}_{d,i}=0 \\ \left[\displaystyle\sum_{k'=-Q_{\bar{\Delta},i}}^{Q_i+Q_{\bar{\Delta},i}-1}\sum_{f=1}^{N_f}\underline{W}_n^{d,k^H}\hat{b}^i_{nQ_i+k'}\hat{\zeta}^i_{f,n}\underline{\hat{Y}}^{i,f}_{k',n}\delta^{k,k'}_{d,i}\right]_{i=N_{\mathrm{TR}}+1}^{N_{\mathrm{TR}}+N_R}=0 \\ \left[\displaystyle\sum_{k'=-Q_{\bar{\Delta},i}}^{Q_i+Q_{\bar{\Delta},i}-1}\underline{W}_n^{d,k^H}\hat{b}^i_{nQ_i+k'}\underline{\hat{Y}}^{i,f}_{k',n}\delta^{k,k'}_{d,i}\right]_{(i,f)=(N_{\mathrm{TR}}+N_R+1,1)}^{(N_{\mathrm{TR}}+N_R+N_D,N_f)}=0 \\ \left[\displaystyle\sum_{f=1}^{N_f}\underline{W}_n^{d,k^H}\hat{\zeta}^i_{f,n}\underline{\hat{Y}}^{i,f}_{k',n}\delta^{k,k'}_{d,i}\right]_{(i,k')=(N_{\mathrm{TR}}+N_R+N_D+1,-Q_{\bar{\Delta},i})}^{(N_{\mathrm{TR}}+N_R+N_D+N_H,Q_i+Q_{\bar{\Delta},i}-1)}=0 \\ \left[\underline{W}_n^{d,k^H}\underline{\hat{Y}}^{i,f}_{k',n}\delta^{k,k'}_{d,i}\right]_{(i,f,k')=(N_{\mathrm{TR}}+N_R+N_D+N_H+1,1,-Q_{\bar{\Delta},i})}^{(NI,N_f,Q_i+Q_{\bar{\Delta},i}-1)}=0 \end{cases} \tag{20}$$

rejection components. Therefore, we introduce the error indicating variables $\xi^i_{k,n}=\hat{b}^{i*}_{k,n}\ b^i_{k,n}$, $\beta^i_{f,n}=\hat{\zeta}^{i*}_{f,n}\zeta^i_{f,n}/\|\hat{\zeta}^i_{f,n}\|^2$, and $\lambda^i_n=\hat{\psi}^{i*}_n\psi^i_n/\|\hat{\psi}^i_n\|^2$, where $(\cdot)^*$ means complex conjugate. $\xi^i_{k,n}$ models the symbol estimation error at previous stage (note that MRC is the initial stage). λ^i_n and $\beta^{i,f}_n$ characterize the power control error and the channel identification error, respectively. $\xi^i_{k,n}$, $\beta^{i,f}_n$, and λ^i_n equal 1 when the estimated data symbol, the estimated channel, and the power control are perfect; otherwise they are complex numbers. In this analysis, we assume that each user's path and its corresponding time-delay has been accurately ascertained (*i.e.*, $\underline{\hat{Y}}^{i,f}_{k,n}=\underline{Y}^{i,f}_{k,n}$). We can rewrite Equation (9) as

$$\begin{aligned}\underline{Y}_n&=\underline{Y}^d_{n,k}+\sum_{i=1}^{NI}\sum_{k'=-Q_{\bar{\Delta},i}}^{Q_i+Q_{\bar{\Delta},i}-1}\sum_{f=1}^{N_f}\psi^i_n b^i_{k',n}\zeta^i_{f,n}\underline{Y}^{i,f}_{k',n}\delta^{k',k}_{d,i}+\underline{N}_n\\&=\underline{Y}^d_{n,k}+\sum_{i=1}^{NI}\sum_{k'=-Q_{\bar{\Delta},i}}^{Q_i+Q_{\bar{\Delta},i}-1}\sum_{f=1}^{N_f}\hat{\psi}^i_n\hat{b}^i_{k',n}\hat{\zeta}^i_{f,n}\xi^i_{k',n}\beta^i_{f,n}\lambda^i_n\underline{\hat{Y}}^{i,f}_{k',n}\delta^{k',k}_{d,i}+\underline{N}_n\\&=\underline{Y}^d_{n,k}+\sum_{i=1}^{NI}\sum_{k'=-Q_{\bar{\Delta},i}}^{Q_i+Q_{\bar{\Delta},i}-1}\sum_{f=1}^{N_f}\xi^i_{k',n}\beta^i_{f,n}\lambda^i_n\underline{\hat{Z}}^{i,f}_{k',n}\delta^{k',k}_{d,i}+\underline{N}_n\end{aligned} \tag{18}$$

The signal after hybrid ISR combining is then

$$\underline{W}_n^{d,k^H}\underline{Y}_n=\frac{\underline{\hat{Y}}^{d\ H}_{k,n}\underline{Y}^d_{k,n}}{\|\underline{\hat{Y}}^d_{k,n}\|^2}s^{d,k}_n+\sum_{i=1}^{NI}\sum_{k'=-Q_{\bar{\Delta},i}}^{Q_i+Q_{\bar{\Delta},i}-1}\sum_{f=1}^{N_f}\xi^i_{k',n}\beta^i_{f,n}\lambda^d_n\underline{W}_n^{d,k^H}\underline{\hat{Z}}^{i,f}_{k',n}\delta^{k',k}_{d,i}+\underline{W}_n^{d,k^H}\underline{N}_n \tag{19}$$

This result allows us to derive the variance of the interference rejection residuals, as shown in the Appendix. There we exploit the expressions for the variance of the channel identification error derived in Reference [18] and for the variance of the power control error derived in Reference [21]. Let $\bar{\psi}^2_d=E[(\psi^d)^2]$ be the average power of the desired user and $\bar{\psi}^2_i$ be the average interference power of user i which varies with the spreading factor and modulation format. The variance of the residual MAI interferences can be written as

$$\mathrm{Var}\left[\delta^{d,k}_{\mathrm{MAI},n}\right]=\frac{1}{L_d}\sum_{\substack{i=1\\ i\neq d}}^{NI}I(\bar{\psi}^2_i,m_i) \tag{21}$$

Copyright © 2008 John Wiley & Sons, Ltd.

DOI: 10.1002/wcm

The interference term $I(\bar{\psi}_i^2, m_i)$ from user i depends on the power of the interferer as well as on the canonic suppression mode m_i applied to this user:

$$I(\bar{\psi}_i^2, m_i) = \begin{cases} \bar{\psi}_i^2 \bar{\kappa}, & m_i = \text{MRC} \\ \bar{\psi}_i^2 \bar{\kappa}\left[(1+\rho_\beta(f_D+\Delta f))(1+\rho_\lambda) - \rho_\xi^{\text{TR}}(f_D+\Delta f)\right], & m_i = \text{TR} \\ \bar{\psi}_i^2 \bar{\kappa}\left[(1+\rho_\beta(f_D)) - \rho_\xi^{R}(f_D)\right], & m_i = \text{R} \\ \bar{\psi}_i^2 \bar{\kappa}\left[1 - \rho_\xi^{D}\right], & m_i = \text{D} \\ \bar{\psi}_i^2 \bar{\kappa}\left[(1+\rho_\beta(f_D)) - 1\right], & m_i = \text{H} \\ 0, & m_i = \text{HD} \end{cases} \tag{22}$$

where f_D and Δf are the maximum Doppler frequency and the carrier frequency offset, respectively. The expressions for the variance of the normalized channel identification error $\rho_\beta(f) = \text{E}[(\beta_{f,n}^i)^2]$, the variance of the power control error $\rho_\lambda = \text{E}[(\lambda_n^i)^2]$, $\rho_\xi^{\text{TR}}(f) = \text{E}_{i,i',k,k',f,f',(i,k,f)\neq(i',k',l')}\left[\xi_{k,n}^i \beta_{f,n}^i \lambda_n^i \xi_{k',n}^{i'*} \beta_{f',n}^{i'*} \lambda_n^{i'}\right]$, $\rho_\xi^R(f) = \text{E}_{k,k',f,f',(k,f)\neq(k',f')}\left[\xi_{k,n}^i \beta_{f,n}^i \xi_{k',n}^{i*} \beta_{f',n}^{i*}\right]$, and $\rho_\xi^D = \text{E}_{k,k',k\neq k'}\left[\xi_{k,n}^i \xi_{k',n}^{i*}\right]$ are derived for a Rayleigh fading channel with P paths to yield

$$\begin{aligned} \rho_\beta(f) &= \frac{P\mu\left(\bar{\kappa}\sigma_N^2 + \text{Var}\left[\delta_{\text{MAI},k,n}^d\right] + \text{Var}\left[\delta_{\text{ISI},k,n}^d\right]\right)}{2\left(1 - \frac{\mu\bar{\psi}_i^2}{2}\right)} \\ &\quad + 2\left[1 - \mathcal{B}_0\left(\frac{2\pi f T_i}{\mu\bar{\psi}_i^2}\right)\right] \\ \rho_\lambda &= \frac{4\pi^2 (f_D \times PC_D)^2}{P-1} \end{aligned} \tag{23}$$

and

$$\begin{aligned} \rho_\xi^{\text{TR}}(f) &= \frac{\rho_\xi\left[MP(NI-1)(Q_i+2Q_{\bar{\Delta},i}+1) + (1+\rho_\lambda)(MP-1)(Q_i+2Q_{\bar{\Delta},i}) + (1+\rho_\lambda)(1+\rho_\beta(f))(Q_i+2Q_{\bar{\Delta},i})\right] + (1+\rho_\lambda)(MP-1)}{NIMP(Q_i+2Q_{\bar{\Delta},i}+1)-1} \\ \rho_\xi^R(f) &= \frac{\rho_\xi\left[(MP-1)(Q_i+2Q_{\bar{\Delta},i}) + (1+\rho_\beta(f))(Q_i+2Q_{\bar{\Delta},i})\right] + MP - 1}{MP(Q_i+2Q_{\bar{\Delta},i}+1)-1} \\ \rho_\xi^D &= \frac{\rho_\xi\left[MP(Q_i+2Q_{\bar{\Delta},i})\right] + MP - 1}{MP(Q_i+2Q_{\bar{\Delta},i}+1)-1} \end{aligned} \tag{24}$$

where $\rho_\xi = (1-(1-\cos(2\pi/\mathcal{M}_i))S_{\text{MRC}}^i)^2$, μ is the channel identification adaptation step-size, $\mathcal{B}_0$ the Bessel function of the first kind of order 0, PC_D the power control feedback delay, and S_{MRC}^i is the symbol error rate after previous stage (we implement MRC combining at the first stage). Equation (22) reveals important characteristics of hybrid ISR. It shows that the variance of the residual MAI interference depends on the detection mode. Indeed, the variance of the interference rejection residuals of the TR mode, $I(\bar{\psi}_i^2, \text{TR})$, is affected by the estimation error of all the channel, power control and data parameters represented by $\rho_\beta(f_D+\Delta f)$, ρ_λ, and $\rho_\xi^{\text{TR}}(f_D+\Delta f)$. The R mode nulls the signal vector of each interferer and hence $I(\bar{\psi}_i^2, R)$ is not affected by neither the power control error (*i.e.*, ρ_λ) nor the carrier frequency offset (*i.e.*, Δf).[¶] The performance of the D mode is not affected by the channel and power estimation errors, but $I(\bar{\psi}_i^2, D)$ depends on the data estimation error specified by ρ_ξ^D. The H mode, unlike the TR, R and D modes, is robust to the data estimation error but its performance deteriorates when the channel estimation error denoted by $\rho_\beta(f_D)$ increases. The HD mode (i.e., *path-by-path* decorrelator) is not affected by imperfect rejection of the interference ($I(\bar{\psi}_i^2, \text{HD}) = 0$), hence its performance is determined by the background noise. It follows from Equation (23) that $\rho_\beta(f)$ is dependent on the noise and residual interference variance. Due to the analytical complexity of the problem, we have resorted to a worst case analysis for which we have $\text{Var}\left[\delta_{\text{MAI},k,n}^d\right] + \text{Var}\left[\delta_{\text{ISI},k,n}^d\right] = \frac{1}{L_d}\sum_{\substack{i=1 \\ i\neq d}}^{NI} \bar{\psi}_i^2$. This amounts to assuming that all the users are detected by simple MRC.

[¶] We assume here that the frequency offset is small compared to the observation interval.

Copyright © 2008 John Wiley & Sons, Ltd.

DOI: 10.1002/wcm

Hence the gains due to interference rejection are not taken into account when evaluating the channel identification error, and $\rho_\beta(f)$ becomes

$$\rho_\beta(f) = \frac{P\mu\left(\bar{\kappa}\sigma_N^2 + \frac{\bar{\kappa}}{L_d}\sum_{\substack{i=1\\ i\neq d}}^{NI}\bar{\psi}_i^2\right)}{2\left(1-\frac{\mu\bar{\psi}_i^2}{2}\right)} + 2\left[1-\mathcal{B}_0\left(\frac{2\pi f T_i}{\mu\bar{\psi}_i^2}\right)\right] \tag{25}$$

The variances of the residual ISI interferences can be written as

$$\mathrm{Var}\left[\delta_{\mathrm{ISI},n}^{d,k}\right] = I\left(\bar{\psi}_d^2, m_d\right)\left(\bar{\kappa}-1+\delta_{is}\right)/\bar{\kappa} \tag{26}$$

where $\delta_{is}(0 \le \delta_{is} < 1)$ is a measure of the relative impact of the interference generated by the other paths on a given path of the desired user [17]. The SNR of the desired user can be estimated as

$$\mathrm{SNR}_{\mathrm{ISR}}^d = \frac{M\bar{\psi}_d^2}{\mathrm{Var}\left[\delta_{\mathrm{MAI},k,n}^d\right] + \mathrm{Var}\left[\delta_{\mathrm{ISI},k,n}^d\right] + \bar{\kappa}\sigma_N^2} \tag{27}$$

The BER performance of the dth user's hybrid ISR receiver is then given as follows:

$$P_e^d = \Omega(\mathrm{SIR}_{\mathrm{ISR}}^d) \tag{28}$$

where Ω represents the single-user bound (SUB), which is classically defined as a conditional Gaussian Q-function over ψ_d and ψ_i. When using this classical representation, the average BER is derived by first finding the pdfs of ψ_d and ψ_i and then averaging over those pdfs. Since it is difficult to find a simple expression for the pdfs of ψ_d and ψ_i, we may consider an approximative pdf. In this analysis, we choose to simulate Ω without imposing any pdf approximation.

The link-level performance analysis leads to a fundamental insight into the hybrid ISR mechanisms. It confirms that hybrid ISR performance varies from user to user and depends on a wide variety of factors such as the detection mode, the propagation environment (data, channel, and power control estimation errors), and the strength of the background noise. It also shows that we should assign more robust modes to the groups of users that generate higher transmission power to improve the overall performance of the system. In multi-rate transmission, all the users (and especially the low-power users) require increased protection against the strong interference of the high-power users. Therefore, increasing the robustness of the detection mode of the group of high-power users will reduce the residual interference of all users.

To validate the link-level performance analysis, we consider a dual-rate system and the combination of the TR and R, D, or H modes in hybrid ISR. We select the setup that will be introduced in Section 5. We also assume a frequency offset $\Delta f = 200$ Hz (*i.e.*, about 0.1 ppm). The users targeted for suppression are split into two groups, a larger number of N_l users with low data rate and a smaller number of N_h users with high data-rate. The hybrid TR/R and TR/H modes null the low data-rate groups with the canonic TR mode and they null the high data-rate users with the canonic R and H modes, respectively. The multi-rate environment is simulated with $N_l = 20$ BPSK users and $N_h = 10$ 8PSK users with spreading factors of $L = 128$ and $L = 32$, corresponding to transmission rates of 30 Kb/s and 360 Kb/s, respectively. In Figure 2(a), we plot the link-level performance of both BPSK and 8PSK users with the hybrid TR/R and TR/H modes along with the canonic TR, R, D, and H modes. It is seen that there is in general a very good match between the analytical and simulation results. The impact of the number of high-rate users and their spreading factor on the accuracy of the analytical analysis is illustrated in Figure 2(b) and (c). It is seen, not surprisingly, that the GA is less accurate when the number of users and/or the spreading factor are low. To illustrate the impact of speed on the performance analysis, we illustrate in Figure 2(d) the link-level performance of both BPSK and 8PSK users with high Doppler (V = 50 Kmph). Note that the channel estimation error increases with the mobile speed. Since our performance analysis considers the channel estimation error, there is a very good match between the analytical and simulation results.

To the best of our knowledge, this is the most general CDMA link-level performance analysis available in the literature. Indeed it takes into account data, channel and power control errors, holds for multi-rate transmissions and MUD, and applies to the MRC receiver and the *path-by-path* decorrelator.

4.2. Link-Level Performance Analysis of PIC Technique

For comparison purposes, we also analyze as an additional contribution the link-level performance of the parallel interference cancellation (PIC) technique.

Copyright © 2008 John Wiley & Sons, Ltd.

DOI: 10.1002/wcm

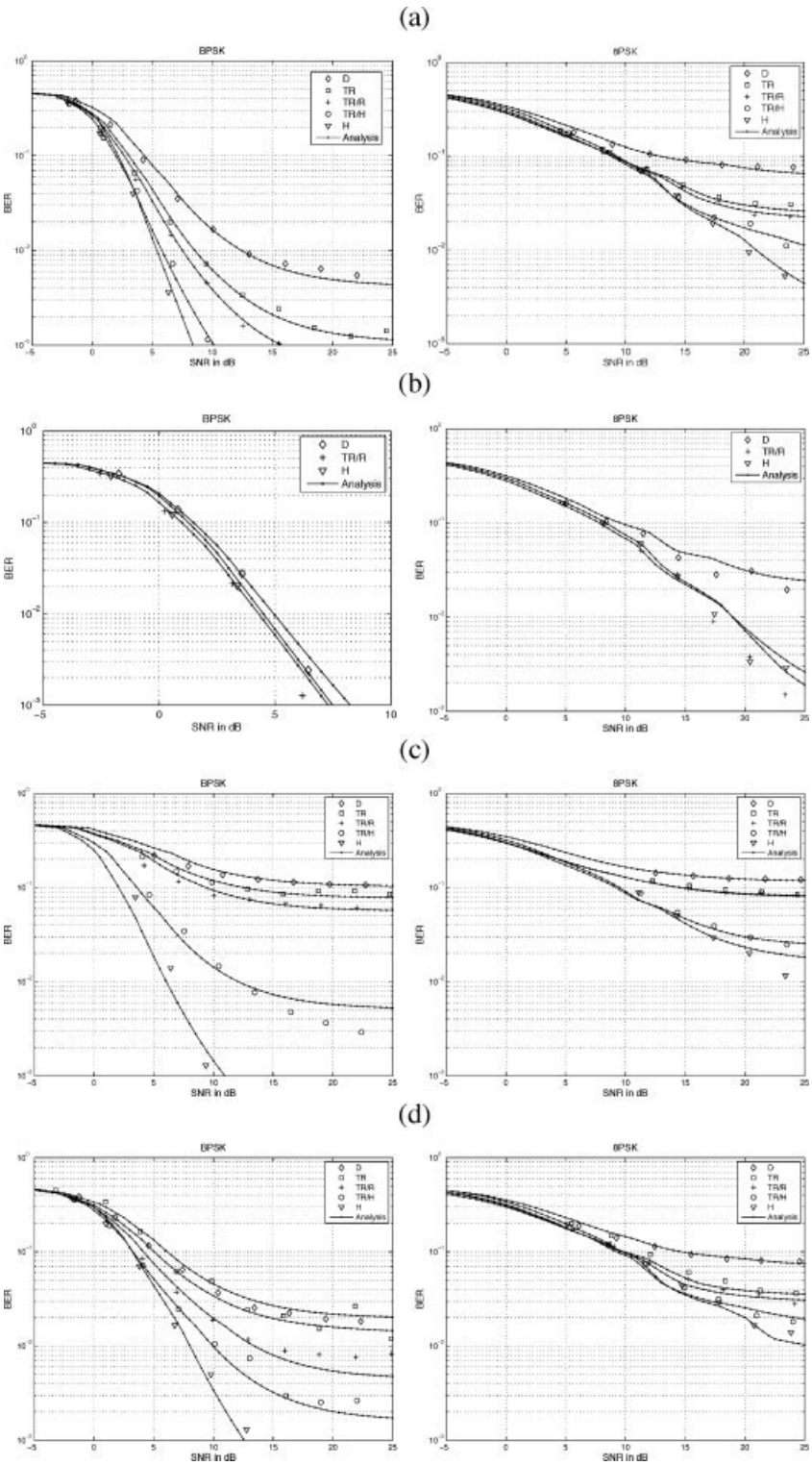

Fig. 2. BER versus SNR in dB for BPSK and 8PSK users with different setups: (a) 10 high-rate users (8PSK, $L = 32$), 20 low-rate users (BPSK, $L = 128$), and the speed $V = 5$ km/h, (b) 2 high-rate users (8PSK, $L = 32$), 20 low-rate users (BPSK, $L = 128$), and the speed $V = 5$ km/h, (c) 10 high-rate users (8PSK, $L = 16$), 20 low-rate users (BPSK, $L = 128$), and the speed $V = 5$ km/h, and (d) 10 high-rate users (8PSK, $L = 32$), 20 low-rate users (BPSK, $L = 128$) and the speed $V = 50$ km/h.

Copyright © 2008 John Wiley & Sons, Ltd.

DOI: 10.1002/wcm

To do so, we derive an expression for the variance of the MAI interference as follows[#]:

$$
\begin{aligned}
I_{\mathrm{MAI}}(\mathrm{PIC}) &= \sum_{\substack{i=1\\ i\neq d}}^{NI} \sum_{k=-Q_{\bar{\Delta},i}}^{Q_i+Q_{\bar{\Delta},i}-1} \sum_{f=1}^{N_f} \mathrm{Var}\left(\left(\psi_n^i b_{k,n}^i \zeta_{f,n}^i - \hat{\psi}_n^i \hat{b}_{k,n}^i \hat{\zeta}_{f,n}^i\right) \underline{Y}_{k,n}^{i,f}\right) \\
&= \sum_{\substack{i=1\\ i\neq d}}^{NI} \sum_{k=-Q_{\bar{\Delta},i}}^{Q_i+Q_{\bar{\Delta},i}-1} \sum_{f=1}^{N_f} \mathrm{E}\left[\left(\xi_{k,n}^i \beta_{f,n}^i \lambda_n^i - 1\right)^2\right] \mathrm{Var}\left(\psi_n^i b_{k,n}^i \zeta_{f,n}^i \underline{Y}_{k,n}^{i,f}\right) \\
&= \frac{1}{L_d} \sum_{\substack{i=1\\ i\neq d}}^{NI} \psi_i^2 \mathrm{E}\left[\left(\xi_{k,n}^i \beta_{f,n}^i \lambda_n^i - 1\right)^2\right] \\
&= \frac{1}{L_d} \sum_{\substack{i=1\\ i\neq d}}^{NI} \psi_i^2 \left(1 + [1+\rho_\beta(f_D+\Delta f)][1+\rho_\lambda] - 2\sqrt{\rho_\varepsilon}\right) \qquad (29)
\end{aligned}
$$

Note that when the channel and power control estimation errors approach zero, such that $\rho_\beta(f_D + \Delta f) = \rho_\lambda = 0$, Equation (29) reduces to the following widely used equation (for BPSK modulation) [22]:

$$
\begin{aligned}
I_{\mathrm{MAI}}(\mathrm{PIC}) &= \frac{1}{L_d} \sum_{\substack{i=1\\ i\neq d}}^{NI} \psi_i^2 \left(2 - 2\sqrt{\rho_\varepsilon}\right) \\
&= \frac{1}{L_d} \sum_{\substack{i=1\\ i\neq d}}^{NI} \psi_i^2 \left(4 S_{\mathrm{MRC}}^i\right) \qquad (30)
\end{aligned}
$$

4.3. System-Level Performance Analysis

The general problem we wish to address is how to assign modes to the different groups of users so as to maximize the total multi-cellular system throughput, given an operating condition (*i.e.*, propagation environment, multi-rate distribution). Using the link-level performance analysis established earlier, we will propose a simple computation procedure to evaluate the capacity in terms of number of users per cell for a specific operating condition and mode assignment. The capacity evaluation procedure provides a quick selection of the best mode assignments at specific operating conditions. The intercell interferences are evaluated using the cellular model suggested by Reference [2]. This simple model allows for analytical tractability on one hand, while giving insight into practical systems on the other. The multi-cellular effect on performance is specified by a single parameter, namely the out-cell to in-cell interference ratio [2].

We translate the link-level results into system-level results in terms of total throughput (or spectrum efficiency) under the following four assumptions: (1) All the cells have the same average load of C users per cell. (2) All the cells have the same multi-rate distribution: The C users are divided into G groups, the proportion of users in the group g is denoted r_g (*i.e.*, $\sum_{g=1}^{G} r_g = 1$). (3) Within each group g, all users are received with an equal average power denoted $\bar{\psi}_g^2$. (4) The out-cell to in-cell interference ratio is set to f. Given these assumptions in an interference-limited system (noise is low compared to interference), the signal to interference ratio SIR of the users in the gth group (ignoring ISI for simplicity) is

$$
\mathrm{SIR}_{\mathrm{ISR}}^g = \frac{M\bar{\psi}_g^2}{\frac{1}{L_g}\sum_{\substack{i=1\\ i\neq g}}^{G} Cr_i I(\bar{\psi}_i^2, m_i) + \frac{1}{L_g}(Cr_g - 1) I(\bar{\psi}_g^2, m_g) + \bar{\kappa} f \frac{1}{L_g} \sum_{i=1}^{G} Cr_i \bar{\psi}_i^2} \qquad (31)
$$

The maximum number of users that can access the system can be hence calculated by the simple procedure illustrated in Table II. For a specific operating condition and mode assignment, the capacity evaluation procedure computes the SIR for all groups of users. In a multi-rate system, each group of users has its own required SNR. The quality-of-service constraints on the capacity become

$$
\forall g \in \{1, \ldots, G\}, \quad \mathrm{SIR}_{\mathrm{ISR}}^g \geq \mathrm{SNR}_{\mathrm{req}}^g \qquad (32)
$$

where $\mathrm{SNR}_{\mathrm{req}}^g$ is the required SNR derived from link-level simulations to meet a BER of 5% in order to

[#] In the development of this equation, we consider the properties of the error indicating variables that will be introduced in the Appendix.

Copyright © 2008 John Wiley & Sons, Ltd.

DOI: 10.1002/wcm

Table II. Capacity computation procedure.

1.	Initialize capacity $C = \max\{1/r_g\}$, $g \in \{1, \ldots, G\}$
2.	Start computation loop:
2.1.	Increment capacity $C = C + 0.1$
2.2.	For each group of users $g \in \{1, \ldots, G\}$
	2.2.1. Compute the SIR with MRC $\mathrm{SIR}^g_{\mathrm{MRC}} = \frac{M\bar{\psi}_g^2}{\frac{1}{L_g}\sum_{\substack{i=1\\ i\neq g}}^{G} Cr_i\bar{\psi}_i^2 + \frac{1}{L_g}(Cr_g-1)\bar{\psi}_g^2 + f\frac{1}{L_g}\sum_{i=1}^{G} Cr_i\bar{\psi}_i^2}$
	2.2.2. Compute the symbol error rate SER after MRC stage $S^g_{\mathrm{MRC}} = \Omega(\mathrm{SIR}^g_{\mathrm{MRC}})$
	2.2.3. Compute $\beta^2(f)$, $\rho_\beta(f)$, ρ_λ, $I(\bar{\psi}_g^2, m_g)$
	2.2.4. Compute the SNR $\mathrm{SIR}^g_{\mathrm{ISR}} = \frac{M\bar{\psi}_g^2}{\frac{1}{L_g}\sum_{\substack{i=1\\ i\neq g}}^{G} Cr_i I(\bar{\psi}_i^2, m_i) + \frac{1}{L_g}(Cr_g-1)I(\bar{\psi}_g^2, m_g) + \bar{\kappa} f\frac{1}{L_g}\sum_{i=1}^{G} Cr_i\bar{\psi}_i^2}$
2.3.	if for $\forall g \in \{1, \ldots, G\}$, $\mathrm{SIR}^g_{\mathrm{ISR}} > \mathrm{SNR}^G_{\mathrm{req}}$ go to 2.1, else exit
3.	Decrement capacity $C = C - 0.1$

achieve a QoS of 10^{-6} after channel decoding. After initialization, this procedure increments the capacity C, until the $\mathrm{SIR}^g_{\mathrm{ISR}}$ given by Equation (31) no longer exceeds the required $\mathrm{SNR}^g_{\mathrm{req}}$. C is then reduced to the largest value for which $\forall g \in \{1, \ldots, G\}$, $\mathrm{SIR}^g_{\mathrm{ISR}} \geq \mathrm{SNR}^g_{\mathrm{req}}$. In step 2.2.1, we use the fact that in each group g, all users are received with equal power denoted $\bar{\psi}_g^2$. Hence, the in-cell interference powers before despreading resulting from the $C-1$ in-cell users are $\sum_{\substack{i=1\\ i\neq g}}^{G} Cr_i\bar{\psi}_i^2 + (Cr_g - 1)\bar{\psi}_g^2$. Assuming that the out-cell to in-cell interference ratio is f [2], the total received interference before despreading is $\sum_{\substack{i=1\\ i\neq g}}^{G} Cr_i\bar{\psi}_i^2 + (Cr_g - 1)\bar{\psi}_g^2 + f\sum_{i=1}^{G} Cr_i\bar{\psi}_i^2$. The total interference power is then reduced by the processing gain L_g. In step 2.2.2, we evaluate the symbol error rate S^d_{MRC} after the MRC stage as follows:

$$S^g_{\mathrm{MRC}} = \Omega\left(\mathrm{SIR}^g_{\mathrm{MRC}}\right) \tag{33}$$

where Ω represents the SUB. In step 2.2.3, $\varphi_\beta(f)$ is computed with the worst case of noise and residual interference variance. However, the step-size μ is optimized with respect to the operating conditions to minimize the channel identification error [18]. Thus, the capacity is optimized over μ. This procedure provides a simple performance evaluation tool for each mode assignment,** which allows a quick selection of the best hybrid ISR mode assignments at specific operating conditions.

4.4. Computational Complexity

After we evaluate the total throughput provided by the different mode assignments, we assess their computational complexity in terms of Mops (Million operation per second) per user. In Table I, we provide an estimation of the complexity for different items of ISR. The complexity of the ISR technique is mainly determined by the number of users to be cancelled NI, and the total N_c imposed by the rejection mode. Hence, for a given multi-user system, reducing N_c will reduce the complexity of the detection technique. In wireless communication systems, there is a practical limit to the number of processing operations that can physically be supported. Taking into consideration the complexity limit, we choose the MUD mode that maximizes the total throughput of the system.

5. Simulations

5.1. Simulation Setup

We consider the uplink of a CDMA base station with M antennas operating at a chip rate of 3.840 Mcps and a carrier frequency of 1.9 GHz. The Rayleigh fading channel is frequency selective with 3 equal-power paths. We assume a linear delay drift of 0.07 ppm for each path. We implement closed-loop power control operating at 1600 Hz and adjusting the power in steps of ± 0.5 dB. An error rate on the power control bit of 5% and a feedback delay of $PC_D = 0.625$ ms are

** The number of mode-assignment combinations equals N_m^G, where G is the number of groups of users and N_m is the number of canonic modes (TR, R, D, H). Reducing the total number of combinations is an issue to be addressed in future works.

Copyright © 2008 John Wiley & Sons, Ltd.

DOI: 10.1002/wcm

simulated. All the channel parameters, varying in time, are estimated by the spatio-temporal array-receiver (STAR) [19].

In order to illustrate the mode assignment strategy in a dual-rate environment, we first set a specific scenario (*i.e.*, the out-cell to in-cell interference ratio f, the speed V, the number of receiving antennas M, and the data-rate distribution). After deriving the SUB Ω and the SNR_{req}[††] from BER[‡‡] simulations, we translate these link-level results into system-level results using the capacity evaluation procedure introduced in Section 4.3 for each detection mode. In order to optimize the selection of the MUD mode for multi-rate transmissions, we consider all the possible combinations (cf. footnote 6). We then calculate the complexity per user in Mops, for each detection mode, in order to generate a plot of the total throughput versus the complexity for the different mode assignments. For comparison purposes, we also provide the performance of the PIC technique and the MRC receiver. Note that we assumed that the complexities of PIC and TR mode are comparable.

5.2. Performance Analysis of Hybrid ISR

In the reference simulation setups, we set $f = 0.3$, $V = 5$ km/h, $M = 2$, and data-rate distribution: 80% BPSK users and 20% 8PSK users with spreading factors of $L = 128$ and $L = 32$. The link-level evaluation shows that we should assign more robust modes to the groups of users that generate higher transmission power. This statement reduces the number of combinations to 10 for dual-rate transmission with {TR, R, D, H} possible modes. In addition, we plot the performance of MRC, PIC, and HD (*path-by-path* detector) for comparison purposes. All these combinations are shown in Figure 3(a). We observe that some detection modes, plotted with circles, perform worst than less complex modes. Indeed, even though these modes are able to effectively suppress 8PSK interference despite the channel estimation errors and/or the near-far effect, their performance suffers from noise enhancement. It is therefore inefficient to apply these complex modes in an environment where they do not outperform modes with lower complexity. In order to capture in more detail the impact of some operating conditions, we proceed in Figure 3(b)–(d) to additional comparisons of the performance of different mode assignments with different simulation setups. For simplicity here, we plot the efficient modes only (the modes that perform worst than less complex modes are omitted).

In most situations the simplest modes TR and TR/R provide generally very good performance. They offer an average throughput 100% higher than with MRC. Moreover, TR always outperforms PIC that possess the same level of complexity. Therefore, TR is a very attractive solution in most situations as it combines affordable complexity with satisfactory performance. On the other hand, as performance improves from one mode to another, the complexity required increases while the resulting capacity advantage decreases, making the last capacity gain even more expensive to obtain.

We also notice that pronounced near-far situations make the application of the H mode to the 8PSK users attractive. The advantage of applying the H mode is confirmed in the scenarios where the speed increases ($V = 100$ km/h) or the number of receiving antennas reduces ($M = 1$). Indeed, Figure 3(b) shows that the R/H and H modes outperform all other modes. But when all user modulations are BPSK, the R/H and H modes did not demonstrate a good performance. The reason is that the data rate distribution: 80% (BPSK, $L = 128$) and 20% (BPSK, $L = 32$) presents a moderate near-far situation.

The influence of the channel identification accuracy on the performance of the different detection modes is shown in Figure 3(c). In situations where channel identification is poor due to weak receiver performance (*i.e.*, step-size μ is not optimized), the TR mode provides only 75% gain compared to MRC. However, the D and D/H modes gain interest and achieve a throughput 150% higher than MRC.

In the fourth set of simulations, we assess the impact of the out-cell to in-cell interference ratio f on the performance of hybrid ISR. Hence, we set $f = 0.6$ and $f = 0$. As shown in Figure 3(d), increasing the out-cell to in-cell interference ratio reduces the throughput of the system with all detection modes but the deterioration is more dramatic for the complex modes. The reason is that the out-cell interference in the received signal is scaled by the combiner. This has been shown to result in greater noise

[††] Measured at a BER 5% in order to achieve a QoS of 10^{-6} BER after FEC decoding.

[‡‡] Note that the confidence interval can be derived from the number of bits N_b over which the BER values were calculated as roughly $10/N_b$. The value of N_b is fixed to $N_b = \max\{3000/\text{BER}, 13\,000\}$ in all the simulations.

Copyright © 2008 John Wiley & Sons, Ltd.

DOI: 10.1002/wcm

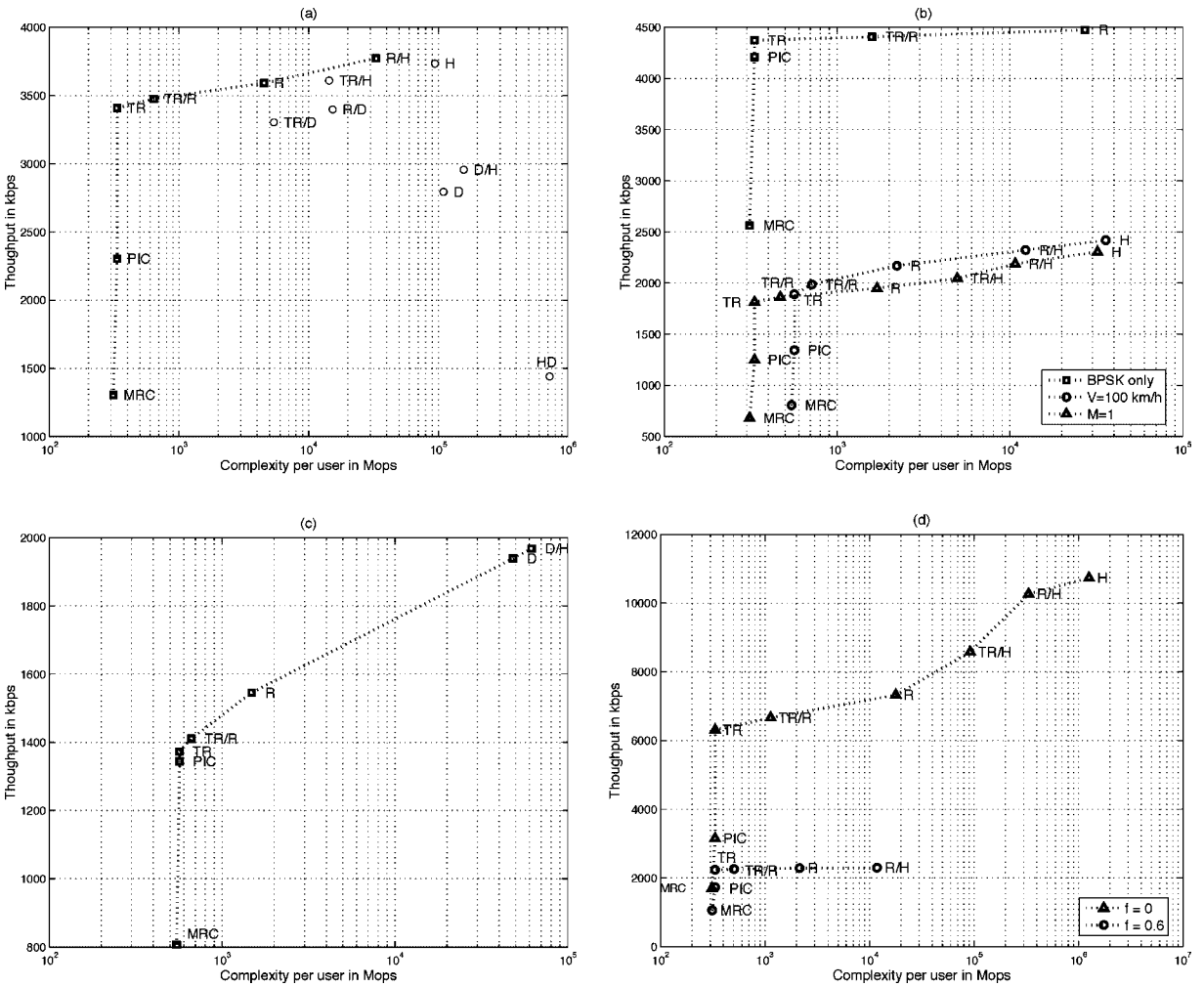

Fig. 3. The total throughput versus the complexity for the different mode assignments in dual-rate environment with different simulation setup: (a) reference simulation setups $R_s \equiv [f = 0.3, V = 5\,\text{km/h}, M = 2$ and data-rate distribution of 20% (BPSK, $L = 128$) and 80% (8PSK, $L = 32)]$, (b) R_s except the data-rate distribution of 20% (BPSK, $L = 128$) and 80% (BPSK, $L = 32$), $V = 100\,\text{km/h}$ or $M = 1$, (c) R_s with poor channel identification (*i.e.*, μ is not optimized), (d) R_s except $f = 0$ or $f = 0.6$.

power because of the noise enhancement phenomenon. Consequently, in the case where the ratio f is large, the background noise is prominent, which makes the complex modes less attractive. This analysis leads to the conclusion suggested in References [14] and [15], that the out-of-cell interference will limit the effectiveness of interference cancellation performed within a single cell. Furthermore, we show that in the realistic situation of non-perfect channel identification, the residual in-cell interference will also limit the performance of the robust detection mode. Note that, since the HD mode is not affected by the imperfect rejection of the interference ($I(\bar{\psi}_i^2, \text{HD}) = 0$), in the case of $f = 0$ its performance is limited by the following fundamental constraint $N_c < MN_P$. In summary, apart from the hypothetic situations where $f = 0$ or channel identification is very poor, the TR mode with complexity of the order of PIC represents the best performance/complexity tradeoff in most situations. In practical scenarios, all modes perform nearly as well in terms of spectrum efficiency or total throughput. It is therefore inefficient to apply complex modes. On the other hand, whenever the use of complex modes (H or D/H) improves significantly the throughput over less complex modes, the complexity required increases rapidly due to the increase in the number of users supported (i.e., both NI and N_c increase) and hence becomes the practical bottleneck.

Copyright © 2008 John Wiley & Sons, Ltd.

DOI: 10.1002/wcm

Note that some of the results regarding the various ISR modes have been shown before in Reference [16]. The key difference is that all the results in Reference [16] were derived via Monte-Carlo simulations. One significant contribution of this paper is the analytical performance analysis. The performance analysis leads to a fundamental insight into the ISR mechanisms and it confirms and qualifies some the ISR properties revealed by time-consuming simulations in a much broader context. Results show that hybrid ISR modes offer a wider range of performance/complexity tradeoffs for multi-rate transmissions. In many operating conditions, the TR/R mode performs almost as well as the R mode but with much less complexity than the R mode.

6. Conclusion

In this contribution, we proposed a hybrid ISR scheme that, instead of suppressing all users with the same canonic ISR mode, splits them into several groups based on their data rates before applying different canonic ISR modes for their nulling. The resulting receiver is well adapted to multi-rate CDMA transmissions with mixed spreading factors and/or modulations (as well as multi-code) and offers a wider range of suppression modes. We analyzed the performance of hybrid ISR in a realistic multi-cellular and multi-rate environment with mixed spreading factors and/or modulations (as well as multi-code). The performance analysis, which is based on the GA and validated by simulations, takes into account data estimation errors, carrier frequency mismatch, imperfect power control, identification errors of time-varying multipath Rayleigh channels, and intercell interference. This analysis enabled us to optimize the selection of the MUD mode for multi-rate transmissions in different operating conditions. The effectiveness of interference cancellation is investigated under different mobile speeds, numbers of receiving antennas, near-far situations, channel estimation errors, and out-cell to in-cell interference ratios. This analysis enabled us to optimize the selection of the MUD mode for multi-rate transmissions in different operating conditions. This investigation leads to the conclusion that because of the out-of-cell interference, the residual in-cell interference, the noise enhancement as well as low mobility, the simplest MUD modes offer the best performance/complexity tradeoff.

Acknowledgement

This work is supported by a Canada Research Chair in High-Speed Wireless Communications and the Strategic Partnership Grants program of NSERC.

Appendix:

Derivation of the Interference Variance

The signal after hybrid ISR combining is given by

$$\underline{W}_n^{d,k^H}\underline{Y}_n = \frac{\hat{\underline{Y}}_{k,n}^{d\ H}\underline{Y}_{k,n}^{d}}{\|\hat{\underline{Y}}_{k,n}^{d}\|^2}s_n^{d,k} + \sum_{i=1}^{NI}\sum_{k'=-Q_{\bar{\Delta},i}}^{Q_i+Q_{\bar{\Delta},i}-1} \times \sum_{f=1}^{N_f}\xi_{k',n}^{i}\beta_{f,n}^{i}\lambda_n^{d}\underline{W}_n^{d,k^H}\hat{\underline{Z}}_{k',n}^{i,f}\delta_{d,i}^{k',k} + \underline{W}_n^{d,k^H}\underline{N}_n \quad (34)$$

Our goal is to estimate the variances $\mathrm{Var}\left[\delta_{\mathrm{MAI},n}^{d,k}\right]$ and $\mathrm{Var}\left[\delta_{\mathrm{ISI},n}^{d,k}\right]$. Since the users are split into several groups and different canonic ISR modes are applied for their nulling, the residual interference from each group can be assumed uncorrelated. Hence, we evaluate the variance of the residual interference of each group individually and then add the variances. Furthermore, we calculate the variance of the residual interference generated by each user separately for all the modes, except for TR, because the hybrid ISR combiner satisfies the optimization property in Equation (20).

Let us consider the general problem of deriving the variance of the sum of random complex variables. We first introduce the variables $x_\alpha, \alpha \in 1, \ldots, N_t$ and $\xi_\alpha, \alpha \in 1, \ldots, N_t$, with the following properties: $\mathrm{E}[\xi_\alpha \xi_{\alpha'}^*] = M_\xi,\ \forall \alpha \neq \alpha',\ \mathrm{E}[\xi_\alpha \xi_\alpha^*] = V_\xi,\ \mathrm{E}[x_\alpha] = 0$, and $\mathrm{Var}[\sum_{\alpha=1}^{N_t} x_\alpha] = 0$. Then we assume that ξ_α and x_α are independent. Thus we derive the variance as follows:

$$\mathrm{Var}\left[\sum_{\alpha=1}^{N_t}\xi_\alpha x_\alpha\right] = \sum_{\alpha=1}^{N_t}\mathrm{Var}[\xi_\alpha x_\alpha] + \sum_{\alpha=1}^{N_t}\sum_{\alpha'=1\alpha'\neq\alpha}^{N_t}\mathrm{E}[\xi_\alpha \xi_{\alpha'} x_\alpha x_{\alpha'}]$$

Copyright © 2008 John Wiley & Sons, Ltd.

DOI: 10.1002/wcm

$$= \sum_{\alpha=1}^{N_t} V_\xi \mathrm{Var}[x_\alpha] + \sum_{\alpha=1}^{N_t} \sum_{\alpha'=1\alpha'\neq\alpha}^{N_t} \mathrm{E}[\xi_\alpha \xi_{\alpha'}]\mathrm{E}[x_\alpha x_{\alpha'}]$$
$$= \sum_{\alpha=1}^{N_t} V_\xi \mathrm{Var}[x_\alpha] + \sum_{\alpha=1}^{N_t} \sum_{\alpha'=1\alpha'\neq\alpha}^{N_t} M_\xi \mathrm{E}[x_\alpha x_{\alpha'}] \quad (35)$$

From $\mathrm{Var}[\sum_{\alpha=1}^{N_t} x_\alpha] = 0$ we have

$$\mathrm{Var}\left[\sum_{\alpha=1}^{N_t} x_\alpha\right] = \sum_{\alpha=1}^{N_t} \mathrm{Var}[x_\alpha] + \sum_{\alpha=1}^{N_t} \sum_{\alpha'=1\alpha'\neq\alpha}^{N_t} \mathrm{E}[x_\alpha x_{\alpha'}] = 0$$
$$\Rightarrow \sum_{\alpha=1}^{N_t} \sum_{\alpha'=1\alpha'\neq\alpha}^{N_t} \mathrm{E}[x_\alpha x_{\alpha'}] = -\sum_{\alpha=1}^{N_t} \mathrm{Var}[x_\alpha] \quad (36)$$

Then, by replacing Equation (36) in Equation (35) we obtain

$$\mathrm{Var}\left[\sum_{\alpha=1}^{N_t} \xi_\alpha x_\alpha\right] = (V_\xi - M_\xi) \sum_{\alpha=1}^{N_t} \mathrm{Var}[x_\alpha] \quad (37)$$

Now we apply the same procedure to derive the variance of the residual interference of each group. The hybrid ISR combiner $\underline{W}_n^{d,k}$ satisfies the optimization property in Equation (20), thus

$$\begin{cases} \mathrm{Var}\left[\sum_{i=1}^{N_{\mathrm{TR}}} \sum_{k'=-Q_{\bar{\Delta},i}}^{Q_i+Q_{\bar{\Delta},i}-1} \sum_{f=1}^{N_f} \underline{W}_n^{d,k^H} \underline{\hat{Z}}_{k',n}^{i,f} \delta_{d,i}^{k,k'}\right] = 0 \\ \mathrm{Var}\left[\lambda_n^i \sum_{k'=-Q_{\bar{\Delta},i}}^{Q_i+Q_{\bar{\Delta},i}-1} \sum_{f=1}^{N_f} \underline{W}_n^{d,k^H} \underline{\hat{Z}}_{k',n}^{i,f} \delta_{d,i}^{k,k'}\right]_{i=N_{\mathrm{TR}}+1}^{N_{\mathrm{TR}}+N_R} = 0 \\ \mathrm{Var}\left[\lambda_n^i \beta_{f,n}^i \sum_{k'=-Q_{\bar{\Delta},i}}^{Q_i+Q_{\bar{\Delta},i}-1} \underline{W}_n^{d,k^H} \underline{\hat{Z}}_{k',n}^{i,f} \delta_{d,i}^{k,k'}\right]_{(i,f)=(N_{\mathrm{TR}}+N_R+1,1)}^{(N_{\mathrm{TR}}+N_R+N_D,N_f)} = 0 \\ \mathrm{Var}\left[\lambda_n^i \xi_{k',n}^i \sum_{f=1}^{N_f} \underline{W}_n^{d,k^H} \underline{\hat{Z}}_{k',n}^{i,f} \delta_{d,i}^{k,k'}\right]_{(i,k')=(N_{\mathrm{TR}}+N_R+N_D+1,-Q_{\bar{\Delta},i})}^{(N_{\mathrm{TR}}+N_R+N_D+N_H,Q_i+Q_{\bar{\Delta},i}-1)} = 0 \\ \mathrm{Var}\left[\lambda_n^i \xi_{k',n}^i \beta_{f,n}^i \underline{W}_n^{d,k^H} \underline{\hat{Z}}_{k',n}^{i,f} \delta_{d,i}^{k,k'}\right]_{(i/f/k')=(N_{\mathrm{TR}}+N_R+N_D+N_H+1/1/-Q_{\bar{\Delta},i})}^{(NI,N_f,Q_i+Q_{\bar{\Delta},i}-1)} = 0 \end{cases} \quad (38)$$

We substitute x_α and ξ_α by the corresponding value (see Equation (38)) to derive the variance of the residual interference generated by the different groups of users.

$$\begin{array}{lll} \text{Mode TR}: & x_\alpha = \underline{W}_n^{d,k^H} \underline{\hat{Z}}_{k',n}^{i,f} & \text{and } \xi_\alpha = \xi_{k,n}^i \beta_{f,n}^i \lambda_n^i \\ \text{Mode R}: & x_\alpha = \underline{W}_n^{d,k^H} \lambda_n^i \underline{\hat{Z}}_{k',n}^{i,f} & \text{and } \xi_\alpha = \xi_{k,n}^i \beta_{f,n}^i \\ \text{Mode D}: & x_\alpha = \underline{W}_n^{d,k^H} \lambda_n^i \beta_{f,n}^i \underline{\hat{Z}}_{k',n}^{i,f} & \text{and } \xi_\alpha = \xi_{k,n}^i \\ \text{Mode H}: & x_\alpha = \underline{W}_n^{d,k^H} \lambda_n^i \xi_{k',n}^i \underline{\hat{Z}}_{k',n}^{i,f} & \text{and } \xi_\alpha = \beta_{f,n}^i \\ \text{Mode HD}: & x_\alpha = \underline{W}_n^{d,k^H} \lambda_n^i \xi_{k',n}^i \beta_{f,n}^i \underline{\hat{Z}}_{k',n}^{i,f} & \text{and } \xi_\alpha = 1 \end{array} \quad (39)$$

In the following, we will derive the value of V_ξ^{TR} and M_ξ^{TR} for the group detected by the TR mode under the following three assumptions: (1) All the error indicating variables $\xi_{k,n}^i$, $\beta_{f,n}^i$, and λ_n^i are independent. (2) All the random sequence variables $(\xi_{k,n}^i)$'s, $(\beta_{f,n}^i)$'s, and (λ_n^i)'s are independent and identically distributed. (3) $\mathrm{E}[\beta_{f,n}^i] = \mathrm{E}[\lambda_n^i] = 1$. Given these assumptions we derive V_ξ^{TR} as follows:

$$\begin{aligned} V_\xi^{\mathrm{TR}} &= \mathrm{E}\left[\xi_{k,n}^i \beta_{f,n}^i \lambda_n^i \xi_{k,n}^{i*} \beta_{f,n}^{i*} \lambda_n^{i*}\right] \\ &= \mathrm{E}\left[\xi_{k,n}^i \xi_{k,n}^{i*}\right] \mathrm{E}\left[\beta_{f,n}^i \beta_{f,n}^{i*}\right] \mathrm{E}\left[\lambda_n^i \lambda_n^{i*}\right] \\ &= \mathrm{E}\left[\beta_{f,n}^i \beta_{f,n}^{i*}\right] \mathrm{E}\left[\lambda_n^i \lambda_n^{i*}\right] \\ &= \left[1 + \rho_\beta(f_D + \Delta f)\right][1 + \rho_\lambda] \end{aligned} \quad (40)$$

In order to evaluate V_ξ^{TR}, we exploit the expression for the variance of the channel identification error in Reference [18] and the variance of the power control error in Reference [21]. Hence, $\rho_\beta(f) = \frac{1}{\mathrm{mean}_f \|\hat{\xi}_{f,n}^i\|^2} \times \beta^2(f) = P \times \beta^2(f)$, where $\beta^2(f)$ is defined in Equation (1.47) in Reference [18], and ρ_λ varies with the Doppler frequency f_D (Equation (51)

Copyright © 2008 John Wiley & Sons, Ltd.

DOI: 10.1002/wcm

in Reference [21]), yielding

$$\rho_\beta(f) = \frac{P\mu\left(\bar{\kappa}\sigma_N^2 + \mathrm{Var}\left[\delta^d_{\mathrm{MAI},k,n}\right] + \mathrm{Var}\left[\delta^d_{\mathrm{ISI},k,n}\right]\right)}{2\left(1 - \frac{\mu\bar{\psi}_i^2}{2}\right)} + 2\left[1 - \mathcal{B}_0\left(\frac{2\pi f T_i}{\mu\bar{\psi}_i^2}\right)\right]$$

$$\rho_\lambda = \frac{4\pi^2(f_D \times PC_D)^2}{P-1} \tag{41}$$

where μ is the channel identification adaptation step-size, $\mathcal{B}_0$ is the Bessel function of the first kind of order 0, and PC_D is the power control feedback delay. Below we derive the expectation $M_\xi^{\mathrm{TR}} = \mathrm{E}_{i,i',k,k',f,f',(i,k,f)\neq(i',k',l')}[\xi^i_{k,n}\beta^i_{f,n}\lambda^i_n\xi^{i'*}_{k',n'}\beta^{i'*}_{f',n}\lambda^{i'}_n]$. Since we have

$$M_\xi^{\mathrm{TR}} = \begin{cases} \mathrm{E}\left[\xi^i_{k,n}\xi^{i'*}_{k',n}\right] = \mathrm{E}\left[\xi^i_{k,n}\right]^2, & i' \neq i \\ \mathrm{E}\left[\xi^i_{k,n}\right]^2[1+\rho_\lambda], & i' = i, k' \neq k,\ f' \neq f \\ \mathrm{E}\left[\xi^i_{k,n}\right]^2[1+\rho_\beta(f_D+\Delta f)][1+\rho_\lambda], & i' = i,\ k' \neq k,\ f' = f \\ 1+\rho_\lambda, & i' = i, k' = k,\ f' \neq f \end{cases} \tag{42}$$

the value M_ξ will be the weighted average $\rho_\xi^{\mathrm{TR}}(f_D + \Delta f)$ where

$$\rho_\xi^{\mathrm{TR}}(f) = \frac{\rho_\xi\left[MP(NI-1)(Q_i+2Q_{\tilde{\Delta},i}+1) + (1+\rho_\lambda)(MP-1)(Q_i+2Q_{\tilde{\Delta},i}) + (1+\rho_\lambda)(1+\rho_\beta(f))(Q_i+2Q_{\tilde{\Delta},i}) + (1+\rho_\lambda)(MP-1)\right]}{NI \times MP(Q_i+2Q_{\tilde{\Delta},i}+1) - 1} \tag{43}$$

If the symbol error rate after the previous stage $S^i_{\mathrm{MRC}} \ll 1$ (we implement an MRC combining at the first stage), the value of $\rho_\xi = \mathrm{E}[\xi^i_{k,n}]^2$ can be derived as follows [17]:

$$\rho_\xi = \left(1 - (1 - \cos(2\pi/\mathcal{M}_i))S^i_{\mathrm{MRC}}\right)^2 \tag{44}$$

The variance of the residual interference generated by all users in the group detected by the canonic mode TR is

$$I(\mathrm{TR}) = \left(V_\xi^{\mathrm{TR}} - \rho_\xi^{\mathrm{TR}}(f_D+\Delta f)\right)\sum_{i=1}^{N_{\mathrm{TR}}}\sum_{k=-Q_{\tilde{\Delta},i}}^{Q_i+Q_{\tilde{\Delta},i}-1} \times \sum_{f=1}^{N_f}\mathrm{Var}\left(\psi^i_n b^i_{k,n}\zeta^i_{f,n}\underline{W}_n^{d,k^H}\underline{\hat{Y}}^{i,f}_{k,n}\right) \tag{45}$$

We now assume that the combiner $\underline{W}_n^{d,k}$ and $\psi^i_n b^i_{k,n}\zeta^i_{f,n}\underline{\hat{Y}}^{i,f}_{n,k}$ are uncorrelated. We also consider that $\mathrm{E}[\|\underline{W}_n^{d,k}\|^2] = \bar{\kappa}$, which is a measure of the enhancement of the white noise compared to the MRC combiner [17]. Hence the variance of the residual interference from the group TR can be written as

$$I(\mathrm{TR}) = \frac{1}{L_d}\left(V_\xi^{\mathrm{TR}} - \rho_\xi^{\mathrm{TR}}(f_D+\Delta f)\right)\bar{\kappa}\sum_{i=1}^{NI}\bar{\psi}_i^2 = \frac{1}{L_d}\sum_{i=1}^{NI} I(\bar{\psi}_i^2, \mathrm{TR}) \tag{46}$$

where L_d is the spreading factor of the desired user. In the developments of Equation (46) above, we exploited the expression for the variance of the interference derived in Reference [23]. However, we introduced a correction factor of 3/2 because we consider practical square-root raised cosine pulses. Indeed, the performance evaluation with a rectangular pulse shape leads to an overestimation of the system capacity by $\frac{3(1-R/4)}{2}$ relative to the evaluation which uses the square-root raised cosine filter with a roll-off factor of R [24]. In order to derive the variance of the residual interference of the groups of users detected by the modes R, D and H, we calculate the variance of the interference generated by each user separately. First, we substitute x_α and ξ_α by the corresponding value (see Equation (38)). Then we follow the same procedure as for the TR mode. It is important to mention here that

Copyright © 2008 John Wiley & Sons, Ltd.

DOI: 10.1002/wcm

there is no effect of the carrier frequency offset (CFO) on the amount of residual interference for the R, D, and H modes. Indeed the combiner $\underline{W}^{d,k^H}$ satisfies the optimization property in Equation (20). Thus it is not affected by the CFO of other users[§§], *i.e.*,

$$\forall\, i \neq d,\ \ \underline{W}_n^{d,k^H}\,\underline{\hat{Y}}_n^i = 0 \implies \underline{W}_n^{d,k^H} e^{2\pi\Delta f^i n T_P}\,\underline{\hat{Y}}_n^i = 0 \tag{47}$$

References

1. Hou J, Smee JE, Pfister HD, Tomasin S. Implementing interference cancellation to increase the EV-DO Rev A reverse link capacity. *IEEE Communications Magazine* 2006; **44**(2): 96–102.
2. Rappaport TS. *Wireless Commmunications: Principles & Practice*. Prentice Hall PTR: Upper Saddle River, NJ, 1999.
3. Mitra U. Comparaison of maximum-likelihood-based detection for two multirate access schemes for CDMA signals. *IEEE Transactions on Communications* 1999; **47**(1): 64–77.
4. Saquib M, Yates R, Mandayam N. Decorrelating detectors for a dual rate synchronous DS/CDMA system. *IEEE VTC 1996* 1996; 377–381.
5. Sabharwal A, Mitra U, Moses R. MMSE receivers for multirate DS-CDMA systems. *IEEE Transactions on Communications* 2001; **49**(12): 2184–2197.
6. Johansson AL, Svensson A. On multirate DS/CDMA schemes with interference cancellation. *Journal Wireless Personal Communications* 1999; **9**: 1–9.
7. Han SH, Lee JH. Multi-stage partial PIC receivers for multi-rate DS-CDMA system with multiple modulation. *IEEE WCNC 2003* 2003, **1**: 591–594.
8. Guo Z, Letaief KB. Performance of multiuser detection in multirate DS-CDMA systems. *IEEE Transactions on Communications* 2003; **51**(12): 1979–1983.
9. Jutti MJ. Multiuser detector performance comparaisons in multirate CDMA systems. *IEEE VTC 1998* 1998; **1**: 31–35.
10. Abrao T, Jeszensky PJE. Multistage hybrid interference canceller for asynchronous multirate DS-CDMA systems in AWGN and flat Rayleigh channels. *IEEE International Symposium on Spread Spectrum 2002*; 283–287.
11. Han SH, Lee JH. Group-wise successive interference cancellation receiver with adaptive MMSE detection for dual-rate DS-CDMA system. *IEEE GLOBECOM 2002* 2002; **1**: 514–518.
12. Guo D, Rasmussen LK, Lim TJ. Linear parallel interference cancellation in long-code CDMA multiuser detection. *IEEE Journal on Selected Areas in Communications* 1999; **17**(12): 2074–2081.
13. Zaidel BM, Shamai S, Verdu S. Multicell uplink spectral efficiency of coded DS-CDMA with random signatures. *IEEE Journal on Selected Areas in Communications* 2001; **19**(8): 1556–1569.
14. Saquib M, Yates R. Analysis of a partial decorrelator in a multicell DS-CDMA system. *IEEE Transactions on Communications* 2002; **50**(12): 1895–1898.
15. Agashe P, Woerner BD. Analysis of interference cancellation for a multicellular CDMA environment. *IEEE PIMRC 1995* 1995 **2**: 747–752.
16. Affes S, Hansen H, Mermelstein P. Interference subspace rejection: a framework for multiuser detection in wideband CDMA. *IEEE Journal on Selected Areas in Communications* 2002; **20**(2): 287–302.
17. Hansen H, Affes S, Mermelstein P. Mathematical derivation of interference subspace rejection. *Technical Report*, INRS-EMT, EMT-014-0105, January 2005.
18. Affes S, Mermelstein P. Adaptive space-time processing for wireless CDMA. *Book Chapter, Adaptive Signal Processing: Application to Real-World Problems*, Benesty J, Huang AH (eds). Springer: Berlin, 2003.
19. Cheikhrouhou K, Affes S, Mermelstein P. Impact of synchronization on performance of enhanced array-receivers in wideband CDMA networks. *IEEE Journal on Selected Areas in Communications* 2001; **19**(12): 2462–2476.
20. Madhow U, Honig ML. On the average near-far resistance for MMSE detection of direct sequence CDMA signals with random spreading. *IEEE Transactions on Information Theory* 1999; **45**(6): 2039–2045.
21. Abrardo A, Sennati D. On the analytical evaluation of closed-loop power-control error statistics in DS-CDMA cellular systems. *IEEE Transactions on Vehicular Technology* 2000; **49**(6): 2071–2080.
22. Verdu S. *Multiuser Detection*. Cambridge University Press: Cambridge, UK, 1998.
23. Ottosson T, Svensson A. Multi-rate schemes in DS/CDMA systems. *IEEE VTC 1995* 1995; **2**: 1006–1010.
24. Asano Y, Daido Y, Holtzman J. Performance evaluation for band-limited DS-CDMA communication system. *IEEE VTC 1993* 1993; 464–468.

Authors' Biographies

Besma Smida received the Diplôme d'Ingénieur degree in telecommunications from Ecole Supérieure des Communications de Tunis, Tunisia, in 1995 and the M. Sc. and Ph. D. degrees in telecommunications from INRS-EMT, University of Quebec, Montreal, Canada, in 1998 and 2006. From 1998 to 1999, she worked as a research assistant in the Personal Communications Group of INRS-EMT. From 1999 to 2002, she was a research engineer in the Technology Evolution and Standards group of Microcell Solutions, Montreal, surveying and studying radio-communication technology evolution. She also took part in major wireless normalization committees (3GPP, T1P1).

She is currently a Lecturer at the School of Engineering and Applied Sciences, Harvard University, Cambridge, USA. Her current research interests include multicarrier modulation, Air-to-ground communications, and Satellite and hybrid communications.

She received in 2007 the Gold Medal of the Governor General of Canada and the Excellence Grant of the Director General of INRS.

[§§] We assume here that the frequency offset is small compared to the observation interval.

Copyright © 2008 John Wiley & Sons, Ltd.

DOI: 10.1002/wcm

Sofiène Affes received the Diplôme d'Ingénieur in electrical engineering in 1992, and the Ph.D. degree with honors in signal processing in 1995, both from the École Nationale Supérieure des Télécommunications (ENST), Paris, France.

He has been since with INRS-EMT, University of Quebec, Montreal, Canada, as a Research Associate from 1995 to 1997, then as an Assistant Professor till 2000. Currently he is an Associate Professor in the Wireless Communications Group. His research interests are in wireless communications, statistical signal and array processing, adaptive space-time processing and MIMO. From 1998 to 2002 he has been leading the radio-design and signal processing activities of the Bell/Nortel/NSERC Industrial Research Chair in Personal Communications at INRS-EMT, Montreal, Canada. Currently he is actively involved in a major project in wireless of PROMPT (Partnerships for Research on Microelectronics, Photonics and Telecommunications).

Professor Affes is the co-recipient of the 2002 Prize for Research Excellence of INRS, the recipient of a Discovery Accelerator Supplement award from NSERC since 2008, and holds a Canada Research Chair in Wireless Communications since 2003. He served as a General Co-Chair of the IEEE VTC'2006-Fall conference, Montreal, Canada, and currently acts as a member of Editorial Board of the IEEE Transactions on Wireless Communications and the Wiley Journal on Wireless Communications and Mobile Computing.

Copyright © 2008 John Wiley & Sons, Ltd.

DOI: 10.1002/wcm